

# The Effect of Selenium Nanoparticles on Tramadol Induced Hepatotoxicity in a Rat Model

Arigue A. Dessouky<sup>1</sup>, Manal R. Abd El-haleem<sup>1,3</sup>, Noha Mohamed Halloull<sup>2</sup>, Moustafa M. I. Moustafa<sup>4</sup> and Eman M. Askar<sup>1</sup>

Original  
Article

<sup>1</sup>Department of Medical Histology and Cell Biology, <sup>2</sup>Department of Forensic Medicine and Clinical Toxicology, Faculty of Medicine, Zagazig University, Egypt.

<sup>3</sup>Department of General Histology, Faculty of Dentistry, Egyptian Russian University

<sup>4</sup>Mater hospital, Dublin, Republic of Ireland.

## ABSTRACT

**Introduction:** Selenium nanoparticles (SeNPs) are a promising modality of treatment for various oxidative stress induced and inflammatory diseases. Tramadol (TD) has become the most commonly prescribed opiate with a high liability for addiction, predisposing the liver to oxidative stress induced hepatotoxicity.

**Aim of the Work:** This study aimed to clarify the impact of SeNPs on biochemical and histological alterations induced by TD.

**Materials and Methods:** Sixty rats were divided into four groups: Group I: (Control group) included 15 rats, Group II: (SeNPs group) 5 rats received intraperitoneal (i.p.) injections of SeNPs. Group III: (TD group) 20 rats received i.p. injections of TD. Group IV (SeNPs + TD) 20 rats received SeNPs one hour before each administered dose of tramadol. Liver specimens were carefully harvested and processed for biochemical, light and electron microscopic studies, morphometric and statistical analysis.

**Results:** Tramadol administration resulted in reduced antioxidant enzyme activities and elevated liver enzyme and malondialdehyde levels. Furthermore, dilated congested central veins and sinusoids, swollen hepatocytes with shrunken darkly stained nuclei and rarified cytoplasm, inflammatory infiltrations, and congested portal veins were observed. This was associated with depletion of intracellular glycogen and proteins, increased Bax and Glial fibrillary acidic protein expression, and collagen bundle deposition near hepatic stellate cells, between hepatocytes, and in the spaces of Disse. Administration of SeNPs significantly ameliorated these findings probably due to its antioxidant properties. Biochemically, a significant increase in antioxidant enzyme activities and decrease in liver enzyme and malondialdehyde levels was observed. Liver histology also improved with a significant increase in hepatocyte glycogen and protein content. Additionally, Bax and GFAP expression was comparable to that of the control group.

**Conclusion:** SeNPs were hepatoprotective against oxidative stress induced by TD.

**Received:** 27 June 2021, **Accepted:** 05 August 2021

**Key Words:** Hepatotoxicity; oxidative stress; selenium nanoparticles; tramadol.

**Corresponding Author:** Arigue A. Dessouky, MD, Department of Medical Histology and Cell Biology, Faculty of Medicine, Zagazig University, Egypt, **Tel.:** +20 11 2100 7767, **E-mail:** arigueamir@yahoo.com

**ISSN:** 1110-0559, Vol. 45, No. 4

## INTRODUCTION

Tramadol (TD) is a centrally acting analgesic widely used to alleviate different degrees of pain.<sup>[1]</sup> It exerts its analgesic effect by binding to  $\mu$ -opioid receptors and inhibiting neuronal reuptake of norepinephrine and serotonin.<sup>[2]</sup> Recently, TD has become the most commonly prescribed opiate across the world.<sup>[3]</sup> Tramadol causes desirable euphoric, stimulant, and relaxing effects, resulting in its frequent abuse and subsequent addiction.<sup>[4]</sup> The most common abusers of TD include individuals with previous substance abuse, patients suffering chronic pain, and health professionals.<sup>[5]</sup>

Tramadol is extensively metabolized in the liver by cytochrome P450 (CYP) 2D6 to O-desmethyltramadol (M1), its main active metabolite. M1 is mainly responsible for the  $\mu$ -opioid receptor mediated analgesic effect. It has a 300 times higher binding affinity to  $\mu$ -opioid receptors than

the parent compound.<sup>[6]</sup> This process makes the liver highly susceptible to drug induced hepatotoxicity.<sup>[7]</sup> Tramadol is metabolized and excreted by the liver and kidney, which increases their risk of injury.<sup>[8]</sup> The toxic effects of tramadol on various tissues have also been reported, especially with its long term use in the management of chronic pain.<sup>[9]</sup>

Tramadol as other opiates is known to induce oxidative stress by reducing antioxidant levels.<sup>[10]</sup> Oxidative stress and inflammation are pivotal mechanisms involved in the initiation and progression of liver injury.<sup>[11]</sup> Therefore, antioxidant supplementation may be an effective therapeutic strategy to limit these complications. Selenium is an essential trace element that cannot be synthesized by living organisms and must be obtained from the diet.<sup>[12]</sup> It plays many vital roles in the human body including antioxidant, anti-inflammatory, anti-mutagenic, anti-carcinogenic, anti-viral, anti-bacterial, and anti-fungal

effects.<sup>[13,14]</sup> Selenium exerts its antioxidant role through its incorporation as seleno-cysteine in various enzymes, such as glutathione peroxidase, glutathione reductase, and thioredoxin reductase. It acts as their redox center, which is essential for their biochemical activity. These selenium dependent enzymes are responsible for cellular defense against oxidative stress.<sup>[15]</sup>

The narrow margin between the therapeutic and toxic doses of selenium limit its use.<sup>[16]</sup> SeNPs provide a safer alternative as they are less toxic, more soluble, and provide a higher surface area for antioxidant activity.<sup>[17]</sup> SeNPs have been used in the treatment of various oxidative stress and inflammation mediated disorders e.g. arthritis, cancers, diabetes, and nephropathies. SeNPs have shown efficacy against chemical and pathogen induced liver injury through their antioxidant properties.<sup>[18]</sup> Additionally, SeNPs have shown protective effects against acetaminophen induced hepatic damage<sup>[19,20]</sup> through the improvement of liver function, and reduction of oxidative stress and DNA fragmentation. SeNPs exert their anti-inflammatory effect by attenuating pro-inflammatory cytokine levels through decreasing their gene expression and deactivating nuclear factor kappa-beta.<sup>[21]</sup> SeNPs also impart an anti-apoptotic effect through the reduction of mitochondrial cytochrome-C release, in addition to inhibiting pro-apoptotic and increasing anti-apoptotic protein expression<sup>[22]</sup>.

To the best of our knowledge, no previous studies have been conducted to evaluate the efficacy of SeNPs in mitigating tramadol induced hepatotoxicity. Thus, the aim of this study was to assess the antioxidant effect of SeNPs on the biochemical and histological alterations induced by Tramadol (TD) in the liver.

## MATERIALS AND METHODS

### Chemicals and kits

Tramal (tramadol hydrochloride) 100 mg ampoules were purchased from Mina-pharm Pharmaceutical Company, Cairo, Egypt.

Selenium nanoparticles (30-60 nm) were purchased from Nano-Tech Egypt for Photo-Electronic, 6 October, Cairo, Egypt as a sterilized solution dispersed in phosphate buffered saline (PBS) ready for use (Figure 1).

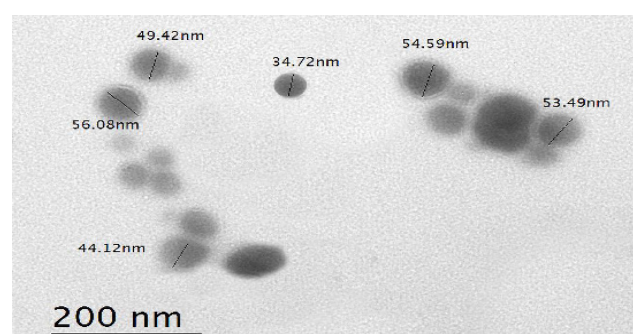


**Fig. 1:** A transmission electron micrograph of the SeNPs displaying their size and shape. The particles are spherical, dispersed regularly in the solution and are not agglomerated. (Mag x 20000)

Kits for determination of alanine transaminase (ALT), aspartate transaminase (AST), alkaline phosphatase (ALP), total proteins and albumin, glutathione peroxidase (GPx), catalase (CAT), superoxide dismutase (SOD), and malondialdehyde (MDA) were purchased from Bio Diagnostics, Inc. (Dokki, Giza, Egypt).

Primary antibodies and secondary antibodies, citrate buffer, the Ultravision Detection System, and Mayer's hematoxylin were purchased from LabVision Thermo Scientific (Fremont, California, USA) for immunohistochemical detection of Bcl2-associated X protein (Bax) for detection of apoptosis (cytoplasmic reaction in the apoptotic hepatocytes) and glial fibrillary acidic protein (GFAP) as an early marker of hepatic stellate cell activation (cytoplasmic reaction in the activated hepatic stellate cells).

### Experimental design

The experimental procedures were approved by the Animal Ethics Committee of Faculty of Medicine Institutional Research Board (MFM IRB: R/16.01.93). The committee adopts the 2013 declaration of Helsinki for research.

The experiment was done on sixty adult male albino rats (180-220 g and 2-3 months of age). These rats were obtained from the animal house of the Faculty of Medicine, Zagazig University. Rats were kept at room temperature with adequate ventilation and a 12 h light/dark cycle and were allowed ad libitum access to food and water throughout the duration of the experiment. Rats were allowed a 1 week adaptation period before the start of the experiment.

### Rats were divided into 4 groups as follows

**Group I (Control group):** (15 rats) which was further subdivided into 3 equal subgroups:

- Subgroup Ia (negative control group); rats received only food and water for 30 days.
- Subgroup Ib (positive control group); rats received daily i.p. injections of 1mL normal saline (vehicle of tramadol) for 30 days.
- Subgroup Ic (positive control group); rats received daily i.p. injections of 1mL phosphate buffered saline (vehicle of SeNPs) for 30 days.

**Group II (SeNPs group):** 5 rats received daily i.p. injections of SeNPs at a dose of 0.5 mg/kg<sup>[19]</sup> for 30 days.

**Group III (TD group):** rats received daily i.p. injections of tramadol at a dose of 20 mg/kg for the first 10 days, 40 mg/kg from the 11th to the 20th day, then 80 mg/kg from the 21<sup>st</sup> to the 30<sup>th</sup> day. All administered doses were given in 1mL of normal saline.<sup>[23]</sup>

**Group IV (SeNPs + TD group):** rats received daily i.p. SeNPs injections at a dose of 0.5 mg/kg<sup>[19]</sup> one hour before each administered dose of tramadol.

The therapeutic dose of TD in human ranges from 50-100 mg every 4-6 hours not to exceed 400 mg/day. In rats, a dose of 40 mg/kg is equivalent to a dose of 421.2 mg in an adult human. The initial dose of 20 mg/kg administered represented the human therapeutic dose, while the 40 and 80 mg/kg doses were given to mimic increasing doses observed in drug abuse.<sup>[24]</sup>

All rats were sacrificed 24 h after the last doses of SeNPs and tramadol. At the end of the experiment, rats were anesthetized with i.p. injection of 40 mg/kg sodium phenobarbital. Blood samples were drawn from the retro-orbital plexus for all groups. Animals were perfused with 2.5% glutaraldehyde and 2% paraformaldehyde in 0.1 M phosphate buffer (pH 7.4) through the left ventricle of the heart. Blood samples were centrifuged and the sera were obtained for biochemical analysis. All animals were sacrificed between 8:00 and 10:00 am to avoid possible diurnal variations in antioxidant enzyme levels. Livers were carefully harvested. The left lobes were frozen in liquid nitrogen, cut into small pieces, and stored at -80°C in preparation for biochemical analysis. The right lobes were processed for light and electron microscope examination.

#### **Biochemical analysis**

Liver homogenates were prepared for measurement of GPx<sup>[25]</sup>, CAT<sup>[26]</sup>, SOD<sup>[27]</sup>, and MDA.<sup>[28]</sup>

Serum ALT, AST, and ALP levels in addition to total proteins and albumin were determined spectrophotometrically following standard procedures.

#### **H&E and histochemical studies**

Specimens for light microscope examination were fixed in 10% buffered formalin and processed to obtain 5µm paraffin sections. The sections were stained with H&E, PAS counterstained with hematoxylin for glycogen demonstration<sup>[29]</sup> and mercuric bromophenol blue<sup>[30]</sup> for intracellular protein detection.

#### **Immunohistochemical studies**

Immunohistochemical staining was done by the avidin biotin complex (ABC) method. 5µm paraffin sections were placed on positively charged slides, deparaffinized, rehydrated, and then incubated in 3% hydrogen peroxide solution in methanol for 10 min to block endogenous peroxidase activity. Sections were then washed in PBS and incubated for 10 min with 10% goat serum at room temperature to block nonspecific binding. Slides were then boiled for 10 min in 10 mmol/L citrate buffer at pH 6 (cat. no. AP 9003) for antigen retrieval, then left to cool for 20 min. Sections were then incubated with two primary mouse monoclonal antibodies: Bax (LabVision Corporation Laboratories, Fremont, California, USA; catalog number MA5- 14003) and GFAP (LabVision Corporation Laboratories Fremont, California, USA; catalog number MS-1376-P) after dilution with PBS (1:1000) and incubated for 30 min at 4°C. Thereafter, sections were washed twice in PBS for 5 min each.

Secondary antibodies (biotinylated goat anti-polyvalent) were applied and sections were incubated again for 20 min, followed by three time washing (for 5 min each) in PBS. Diaminobenzidine tetrahydrochloride solution was applied to the sections and incubated for 10 min.<sup>[29]</sup> Negative control sections were prepared following the same steps after omitting the primary antibodies.

#### **Transmission electron microscope study**

Small pieces of liver from all groups were immediately fixed in 2.5% phosphate buffered glutaraldehyde (pH 7.4) at 4°C for 24 h, rinsed in phosphate buffer, then post-fixed in 1% osmium tetroxide. Specimens were then dehydrated in a series of alcohols, cleared in propylene oxide, and finally embedded in epoxy resin. Blocks were trimmed and sectioned with glass knives by an ultra-microtome. Toluidine blue stained semi-thin sections (1 µm) were examined to select the suitable area for ultra-thin sections. Ultra-thin sections (70-90nm) were stained with uranyl acetate and lead citrate.<sup>[31]</sup> Examination and photography was carried out by Joel JEM 1010 (Jeol Ltd, Tokyo, Japan) in the Electron Microscope Research Laboratory Unit at the Faculty of Agriculture, Mansoura University.

#### **Morphometric analysis**

Slides were examined using the Leica QWin 500 image analyzer computer system (Leica Ltd, Cambridge, UK) at the Image Analysis Unit of the Pathology Department in the Faculty of Dentistry, Cairo University. The mean optical density for PAS, mercuric bromophenol blue, and GFAP immune reaction and the mean area percentage for Bax immunoreaction were quantified by examining ten non overlapping randomly chosen fields in each slide at a magnification of 400. Image analysis was performed by a blind investigator unaware of the experimental procedure.

#### **Statistical analysis**

The collected data were computerized and statistically analyzed using SPSS program (Statistical Package for Social Science) version 25.0. Quantitative data were expressed as mean ± standard deviation (SD). ANOVA F-test was used to calculate difference between quantitative variables in more than two groups in normally distributed data and post hoc LSD test was used for comparing between each two groups. Pearson's correlation coefficient was used to calculate correlation between quantitative variables.  $p < 0.05$  indicated significant results and  $p < 0.001$  indicated highly significant results.

## **RESULTS**

#### **Biochemical results**

No statistically significant differences regarding biochemical markers were detected between the subgroups of the control group (I) or the SeNPs group (II). So, results of subgroup Ia (representing group I) were used for comparison with groups III (TD group) and IV (SeNPs + TD group).

### **Markers of oxidative stress/lipid peroxidation**

TD administration in group III evoked hepatic oxidative stress evidenced by a highly significant reduction ( $p < 0.001$ ) in the activities of the antioxidant enzymes GPx, CAT, and SOD accompanied by a highly significant elevation ( $p < 0.001$ ) in MDA content when compared to the control group (group I). Administration of SeNPs in group IV resulted in a highly significant improvement of these parameters ( $p < 0.001$ ), however, they didn't return to their normal values (Table 1).

### **Liver function tests**

The mean values of serum ALT, AST, and ALP showed a highly significant elevation in group III versus group I rats ( $p < 0.001$ ). Total protein and albumin levels showed a highly significant reduced in group III versus group I ( $p < 0.001$ ). On the other hand, group IV revealed a highly significant lower liver enzyme level and a highly significant increase in protein levels when compared to group III ( $p < 0.001$ ) (Table 2).

### **Histological results**

Histological examination of all subgroup sections of Group I (control group) and Group II (SeNPs group) revealed similar results. Thus, the results of the negative control (subgroup Ia) were used to represent both groups.

### **Light microscope results**

#### **Hematoxylin and Eosin (H&E)**

Examination of H&E stained sections of the control group (I) and SeNPs group (II) revealed the normal hepatic structure. The central veins were surrounded by radiating cords of tightly packed hepatocytes separated by blood sinusoids lined by endothelium. Hepatocytes appeared polyhedral with round vesicular nuclei and stippled acidophilic cytoplasm. Bi-nucleated hepatocytes were also observed (Figure 2a). The portal areas contained portal veins and bile ducts embedded in loose connective tissue (Figure 2b). Group III (TD group) revealed evident alteration of hepatic structures. The central veins and sinusoids appeared dilated and congested (Figures 2c,d,f). Some hepatocytes had vesicular nuclei (Figs. 2c, d & e) while others showed darkly stained nuclei (Figures 2c,d,ef). Some hepatocytes showed slight rarefaction of their cytoplasm (Figure 2c), while others appeared swollen with extensive cytoplasmic rarefaction (Figure 2 f). Bi-nucleated hepatocytes were also observed (Figures 2c,d,e). Inflammatory cells were seen near the central veins (Figure 2d) and in the portal areas (Figures 2ef). Some portal areas contained dilated congested portal veins (Figure 2e) and several bile ducts (Figures 2e,f). Administration of SeNPs with tramadol in group IV led to partial improvement of the hepatic structures. Most hepatocytes had vesicular nuclei and acidophilic cytoplasm with few still showing darkly stained nuclei and vacuolated cytoplasm. Numerous bi-nucleated hepatocytes were seen (Figures 2g,h). The central veins

and sinusoids appeared normal (Figure 2g), while portal areas revealed congested portal veins, bile ducts, and inflammatory cells (Figure 2h).

### **Periodic Acid Schiff**

Periodic Acid Schiff (PAS) stained sections of the control group (group I) and SeNPs group (group II) revealed abundant amounts of glycogen within the hepatocytes around the central veins (Figure 3a) while tramadol administration in group III resulted in a considerable decrease of the glycogen content (Figure 3b). On the other hand, SeNPs administration in group IV lead to an increase in hepatocyte glycogen content (Figure 3c).

### **Mercuric bromophenol blue**

Mercuric bromophenol stained sections of the control group (group I) and SeNPs group (group II) revealed considerable amounts of protein within the hepatocytes (Figure 4a). Treatment with tramadol in group III caused depletion of the protein content within the hepatocytes (Figure 4b), while administration of SeNPs with tramadol in group IV showed hepatocytes with a protein content comparable to that of the control group (Figure 4c).

### **Immunohistochemical results**

#### **Bax immunoexpression**

Bax immune-stained sections of the control group demonstrated a mostly negative cytoplasmic reaction except for a mild positive reaction in few hepatocytes (Figure 5a). Group III (TD group) revealed an intense positive reaction in most hepatocytes (Figure 5b), while a moderate reaction was observed in some group IV (SeNPs + TD group) hepatocytes (Figure 5c).

#### **GFAP immunoexpression**

GFAP immune-stained sections of the control group demonstrated a mild positive reaction in few hepatic stellate cells processes (Figure 6a). Group III (TD group) revealed an intense reaction in both the cells bodies and processes of numerous hepatic stellate cells (Figure 6b), while a moderate reaction was observed in numerous cells in group IV (SeNPs + TD) (Figure 6c).

A highly significant decrease in the optical density of PAS and mercuric bromophenol blue ( $p < 0.001$ ) and a highly significant increase in the mean area % of Bax immuno-expression ( $p < 0.001$ ) and optical density of GFAP ( $p < 0.001$ ) was observed in group III when compared to group I and IV (Table 3). On the other hand, administration of SeNPs with TD in group IV lead to a highly significant increase in optical density of mercuric bromophenol blue ( $p < 0.001$ ) and a highly significant decrease of Bax and GFAP immune expression ( $p < 0.001$ ) when compared to group III (Table 3).

Additionally, a negative Pearson's correlation was observed between antioxidant enzyme activity and Bax and GFAP immune expression. On the other hand, a positive correlation was observed between MDA level and Bax and GFAP immune expression (Table 4).

**Transmission electron microscopy (TEM) results**

Examination of ultra-thin sections of the control group and SeNPs group revealed a normal hepatic ultrastructure. Hepatocytes had round euchromatic nuclei and prominent nucleoli. Their cytoplasm contained numerous mitochondria, rough endoplasmic reticulum, autolysosome, glycogen granules, and lipid droplets (Figure 7a). The adjacent hepatocytes formed the boundaries of the bile canaliculi which contained numerous microvilli. Many hepatocytes had numerous mitochondria and lipid droplets, while few others had electron dense cytoplasm, multivesicular bodies and autophagosomes. Von Kupffer cells with heterochromatic nuclei and dense bodies in their cytoplasm were seen in the sinusoidal lumens. The spaces of Disse contained numerous long microvilli of the hepatocytes (Figure 7b). Hepatic stellate cells were seen in the vicinity of the hepatocytes. They appeared elongated with euchromatic indented nuclei and large fat globules in their cytoplasm. Numerous mitochondria were seen in the hepatocytes (Figure 7c).

Group III (TD group) revealed evident ultrastructural changes. Hepatocytes showed varying degrees of affection. Hepatocytes had dilated rough endoplasmic reticulum, mitochondria with disrupted cristae, and many lipid droplets (Figure 8a). Some nuclei appeared euchromatic

(Figure 8b), others had dilated perinuclear cisternae (Figure 8a), while few appeared ill defined (Figure 8c). The cytoplasm appeared electron dense in some hepatocytes (Figures 8a,b,c,d,e) while others displayed electron lucent cytoplasm (Figures 8a,b). The bile canaliculi contained few microvilli (Figures 8a,c). Von Kupffer cells present in the lumen had pseudopodia, lysosomes, and numerous phagocytic vacuoles (Figure 8b). The spaces of Disse contained few microvilli and collagen fibers (Figures 8c,d). The hepatic stellate cells had numerous long processes (Figure 8d). Some had irregular outline, ill-defined heterochromatic nuclei and numerous marginal vacuoles. Others showed indented euchromatic nuclei and vacuoles in their cytoplasm (Figure 8e). Collagen fibers were observed between the hepatocytes (Figure 8c), in the spaces of Disse (Figures 8c,d), and in the vicinity of the hepatic stellate cells (Figure 8e).

The SeNPs treated group showed improvement of the tramadol induced ultrastructural alterations. Most hepatocytes had euchromatic nuclei, rough endoplasmic reticulum (Figures 9b,c) and numerous intact mitochondria (Figures 9a,b,c); while few had electron dense cytoplasm with lipid droplets (Figures 9a,b). Endothelial cells with euchromatic nuclei with few collagen fiber bundles in their vicinity were seen (Figure 9a).

**Table 1:** Comparison of antioxidant enzyme activities and MDA level in the experimental groups

Variable	Group I (Control group)	Group III (TD group)	Group IV (SeNPs + TD group)	F	p value	LSD
GPx (ng/ml)						
Mean ± SD	19.4 ± 2.0	10.4 ± 1.2	14.8 ± 2.1	120.5	<0.001**	<0.001** <sup>2</sup>
Range	(15.5-21.7)	(8.5-13.2)	(11.7-18.5)			<0.001** <sup>3</sup>
CAT (U/g protein):						
Mean ± SD	81.9 ± 3.4	33.7 ± 3.4	58.9 ± 3.3	1031.6	<0.001**	<0.001** <sup>2</sup>
Range	(77.2-88.6)	(27.6-38.1)	(50.4-62.8)			<0.001** <sup>3</sup>
SOD (U/mg protein):						
Mean ± SD	2.1 ± 0.2	0.9 ± 0.2	1.4 ± 0.4	111.9	<0.001**	<0.001** <sup>2</sup>
Range	(1.9-2.6)	(0.7-1.3)	(0.9-2.0)			<0.001** <sup>3</sup>
MDA (nmol/L):						
Mean ± SD	79.6 ± 8.3	168.1 ± 17.0	106.5 ± 10.70	261.1	<0.001**	<0.001** <sup>2</sup>
Range	(67.5-93.4)	(140.7-194.2)	(91.2-131.2)			<0.001** <sup>3</sup>

a Abbreviations: SD: Standard deviation. F: ANOVA test LSD: Least significant difference  
 b 1: Group I versus Group III 2: Group I versus Group IV 3: Group III versus Group IV  
 \*: Significant (p <0.05) \*\*: Highly significant (p <0.01)

**Table 2:** Comparison of the liver function tests of the experimental groups

Variable \ Group	Group I (Control group)	Group III (TD group)	Group IV (SeNPs + TD group)	F	p value	LSD
ALT (IU/L):						<0.001 <sup>***</sup>
Mean ± SD	31.1 ± 3.1	133.8 ± 14.7	70.7 ± 9.6	503.9	<0.001 <sup>**</sup>	<0.001 <sup>**2</sup>
Range	(25.3-37.1)	(102.5-161.0)	(53.8-84.7)			<0.001 <sup>**3</sup>
AST (IU/L):						<0.001 <sup>**1</sup>
Mean ± SD	65.7 ± 9.1	204.4 ± 21.6	123.6 ± 18.1	331.5	<0.001 <sup>**</sup>	<0.001 <sup>**2</sup>
Range	(49.4-81.7)	(156.3-243.5)	(98.3-162.3)			<0.001 <sup>**3</sup>
ALP (IU/L):						<0.001 <sup>**1</sup>
Mean ± SD	45.9 ± 2.9	81.5 ± 2.9	61.5 ± 2.9	754.3	<0.001 <sup>**</sup>	<0.001 <sup>**2</sup>
Range	(41.6-50.2)	(75.4 – 85.4)	(56.9-66.2)			<0.001 <sup>**3</sup>
T. Protein (g/dl):						<0.001 <sup>**1</sup>
Mean ± SD	7.0 ± 0.5	3.2 ± 0.4	4.6 ± 0.4	391.1	<0.001 <sup>**</sup>	<0.001 <sup>**2</sup>
Range	(5.8-7.8)	(2.5-3.8)	(3.9-5.5)			<0.001 <sup>**3</sup>
Albumin (g/dl):						<0.001 <sup>**1</sup>
Mean ± SD	4.0 ± 0.6	1.9 ± 0.3	2.2 ± 0.5	118.6	<0.001 <sup>**</sup>	<0.001 <sup>**2</sup>
Range	(2.9-4.9)	(1.3-2.4)	(1.3-3.0)			0.04 <sup>*3</sup>

a Abbreviations: SD: Standard deviation. F: ANOVA test LSD: Least significant difference

b 1: Group I versus Group III 2: Group I versus Group IV 3: Group III versus Group IV

\*: Significant ( $p < 0.05$ ) \*\*: Highly significant ( $p < 0.01$ )

**Table 3:** Comparison of the histochemical and immunohistochemical markers in the experimental groups

Variable \ Group	Group I (Control group)	Group III (TD group)	Group IV (SeNPs + TD group)	F	p value	LSD
PAS (optical density)						<0.001 <sup>**1</sup>
Mean ± SD	0.52 ± 0.05	0.31 ± 0.06	0.43 ± 0.03	95.14	<0.001 <sup>**</sup>	<0.001 <sup>**2</sup>
Range	(0.40 – 0.80)	(0.17 – 0.63)	(0.21 – 0.62)			<0.001 <sup>**3</sup>
MBP (optical density)						<0.001 <sup>**1</sup>
Mean ± SD	0.55 ± 0.05	0.12 ± 0.04	0.40 ± 0.05	405.58	<0.001 <sup>**</sup>	<0.001 <sup>**2</sup>
Range	0.46 – 0.63	0.06 – 0.2	0.31 – 0.54			<0.001 <sup>**3</sup>
Bax (area %)						<0.001 <sup>**1</sup>
Mean ± SD	1.05 ± 0.18	5.49 ± 0.67	2.81 ± 0.48	418.76	<0.001 <sup>**</sup>	<0.001 <sup>**2</sup>
Range	0.69 – 1.41	4.23 – 6.53	1.93 – 4.1			<0.001 <sup>**3</sup>
GFAP:(optical density)						<0.001 <sup>**1</sup>
Mean ± SD	0.09 ± 0.03	0.29 ± 0.06	0.21 ± 0.04	93.77	<0.001 <sup>**</sup>	<0.001 <sup>**2</sup>
Range	0.03 – 0.13	0.19 – 0.41	0.03 – 0.41			<0.001 <sup>**3</sup>

a Abbreviations: SD: Standard deviation. F: ANOVA test LSD: Least significant difference

b 1: Group I versus Group III 2: Group I versus Group IV 3: Group III versus Group IV

\*: Significant ( $p < 0.05$ ) \*\*: Highly significant ( $p < 0.01$ )

**Table 4:** Correlation between antioxidant enzyme activities and MDA level with Bax area % immune expression and GFAP optical density of the experimental groups

Variable	Group	Group I (Control group)		Group III (TD group)		Group IV (SeNPs + TD group)	
		Bax area % immune expression	GFAP optical density	Bax area % immune expression	GFAP optical density	Bax area % immune expression	GFAP optical density
MDA	r	-0.088	0.347	0.912 <sup>**</sup>	0.802 <sup>**</sup>	0.041	-0.065
	p	0.712	0.134	<0.001	<0.001	0.864	0.786
GPX	r	-0.190	-0.163	-0.857 <sup>**</sup>	-0.813 <sup>**</sup>	0.452 <sup>*</sup>	-0.295
	p	0.422	0.493	0.001	<0.001	0.045	0.207
CAT	r	0.168	-0.373	-0.953 <sup>**</sup>	-0.857 <sup>**</sup>	-0.116	-0.237
	p	0.478	0.001	<0.001	0.229	0.625	0.314
SOD	r	0.283	-0.018	-0.841 <sup>**</sup>	-0.782 <sup>**</sup>	0.226	0.077
	p	0.226	0.941	<0.001	<0.001	0.339	0.746

\*\* Highly significant correlations

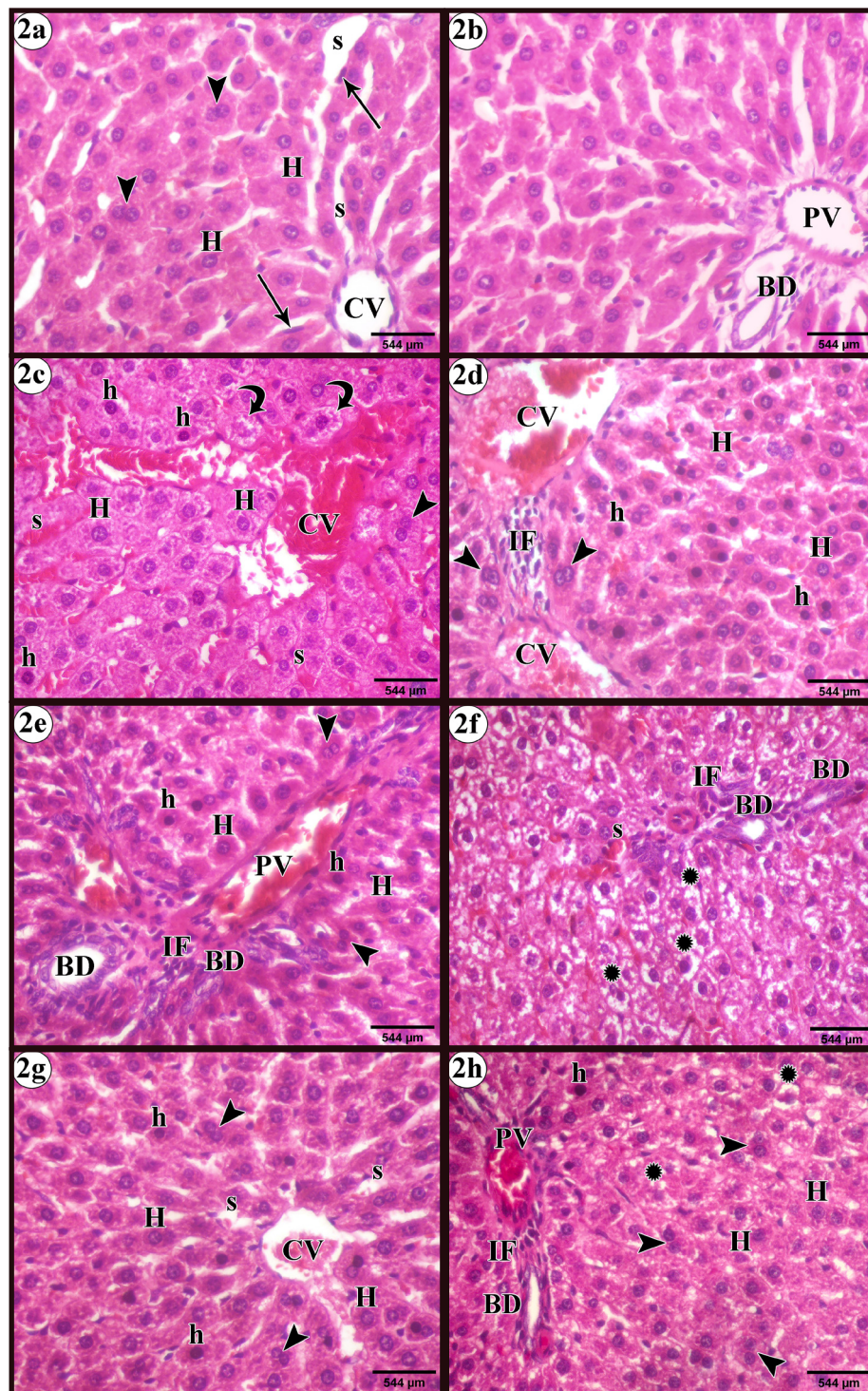


**Fig. 2 (a-h):** Representative photomicrographs of H&E stained sections demonstrating the histological structure of the different groups. Control group (a & b) showing: (a) Central vein (CV) with radiating cords of tightly packed hepatocytes (H). The hepatocytes appear polyhedral with round vesicular nuclei and stippled acidophilic cytoplasm. Blood sinusoids (s) with their endothelial lining (thin arrow) and some binucleated hepatocytes (arrowhead) are also seen. (b) The portal area containing the portal vein (PV) and bile duct (BD). TD group (c-f) showing: (c) Dilated congested central vein (CV) and sinusoids (s). Most hepatocytes have vesicular nuclei (H), while others have darkly stained nuclei (h). Few hepatocytes show slight rarefaction of their cytoplasm (curved arrow). Binucleated hepatocytes (arrowhead) are also observed. (d) Dilated congested central veins (CV) and inflammatory cells (IF). Many hepatocytes have darkly stained nuclei (h), while others have vesicular nuclei (H). Binucleated hepatocytes (arrowhead) are observed. (e) A portal area with dilated congested portal vein (PV), several bile ducts (BD) and inflammatory cells (IF). Some hepatocytes have darkly-stained nuclei (h), with others still demonstrating vesicular nuclei and acidophilic cytoplasm (H). Binucleated hepatocytes (arrowhead) are also observed. (f) Another portal area showing several bile ducts (BD) and inflammatory cells (IF). The adjacent hepatocytes appear swollen with extensive rarefaction of their cytoplasm and shrunken darkly stained nuclei (asterisk). Congested sinusoids (s) are also observed. SeNPs + TD group (g-h) showing: (g) nearly normal appearance of hepatic architecture; most hepatocytes with vesicular nuclei and acidophilic cytoplasm (H) radiating from central vein (CV), blood sinusoids (s) and some binucleated hepatocytes (arrowhead). Few hepatocytes still have darkly stained nuclei (h). Congested portal vein (PV) and bile duct (BD) with few inflammatory cells (IF) are seen. Most hepatocytes show vesicular nuclei and acidophilic cytoplasm (H), while some have darkly stained nuclei (h). Others still appear swollen with rarefied cytoplasm and shrunken darkly stained nuclei (asterisk). Numerous binucleated hepatocytes (arrowhead) can be seen. (Mag. x400)

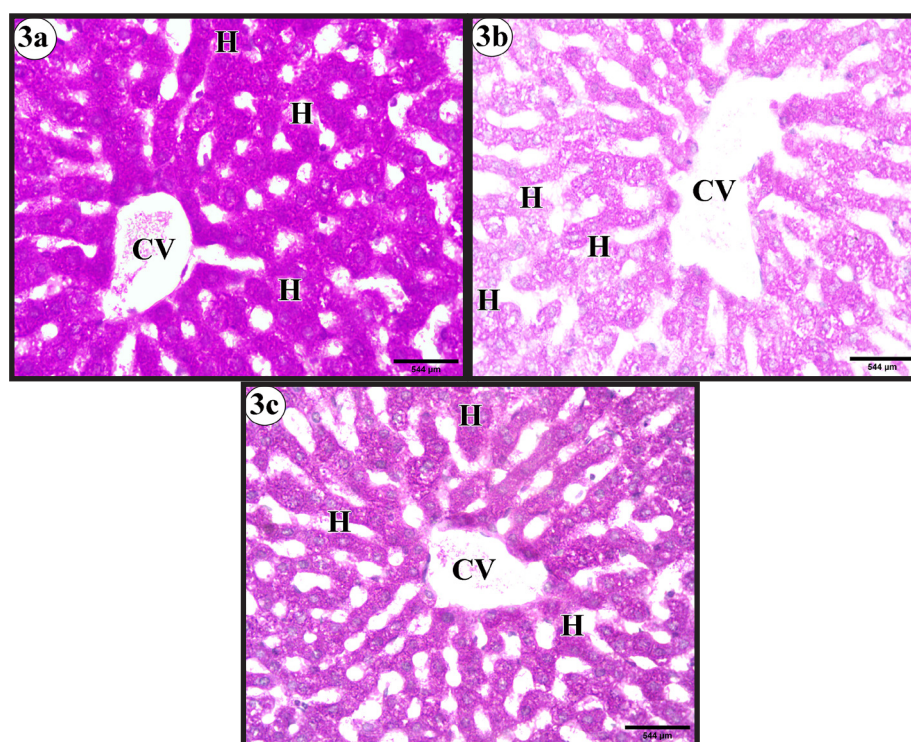


**Fig. 3 (a-c):** Representative photomicrographs of PAS stained sections. (a) Control group: showing abundant glycogen in the hepatocytes. (b) TD group: showing a marked reduction in the glycogen content of hepatocytes. (c) SeNPs + TD group: showing hepatocytes with increased glycogen content. Hepatocytes (H), Central vein (CV). (Mag. x400)

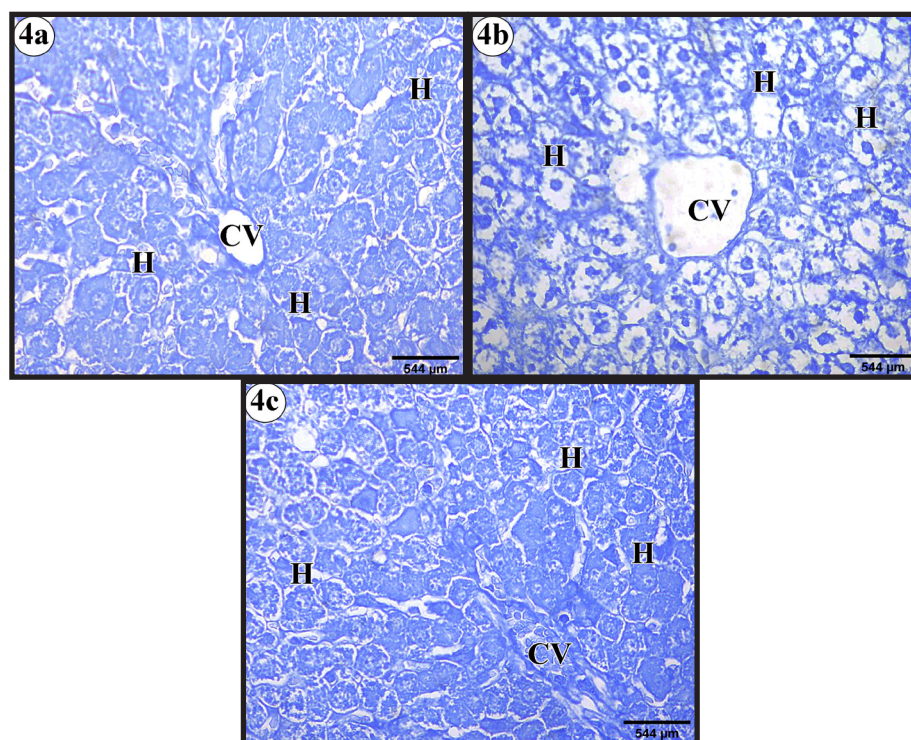


**Fig. 4 (a-c):** Representative photomicrographs of Mercuric bromophenol blue stained sections. (a) Control group: Hepatocytes contain considerable amounts of protein. (b) TD group: Hepatocytes show depletion of their protein content. (c) SeNPs + TD group: Hepatocytes have protein content comparable to that of the control group. Hepatocyte, H. Central vein, CV. (Mag. x400)

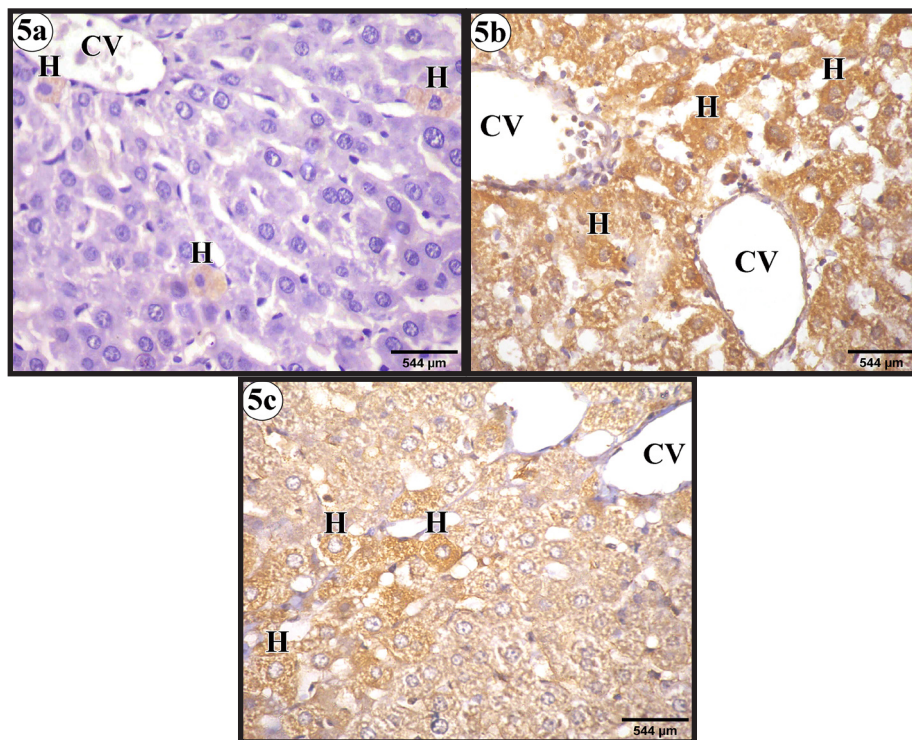


**Fig. 5 (a-c):** Representative photomicrographs of Bax immunoreactivity. (a) Control group: Most hepatocytes show negative reaction except few with mild cytoplasmic immune reaction (b) TD group: Most hepatocytes have intense immune reaction. (c) SeNPs + TD group: Some hepatocytes with a moderate reaction. H, hepatocyte with a positive reaction. CV, central vein. (Mag. x400)

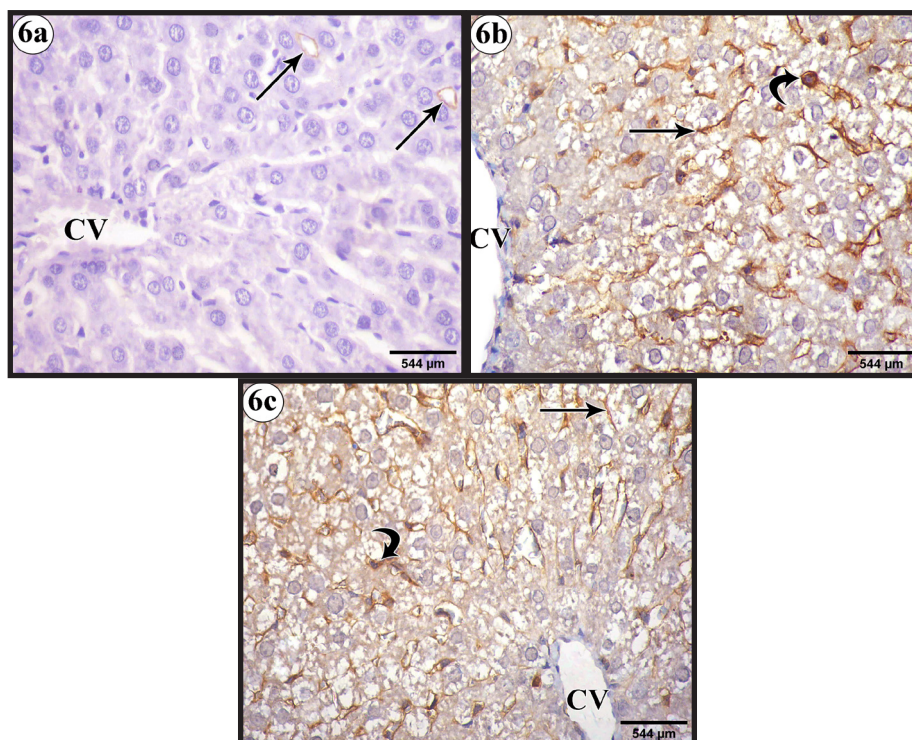


**Fig. 6 (a-c):** Representative photomicrographs of GFAP immunoreactivity. (a) Control group: mild reaction in few hepatic stellate cell processes. (b) TD group: Intense reaction in the cells bodies and processes of numerous hepatic stellate cells. (c) SeNPs + TD group: A moderate reaction in the bodies and processes of hepatic stellate cells is detected. Arrow, positive cytoplasmic reaction in the processes. Curved arrow, positive reaction in the cell bodies. CV, central vein. (Mag. x400)

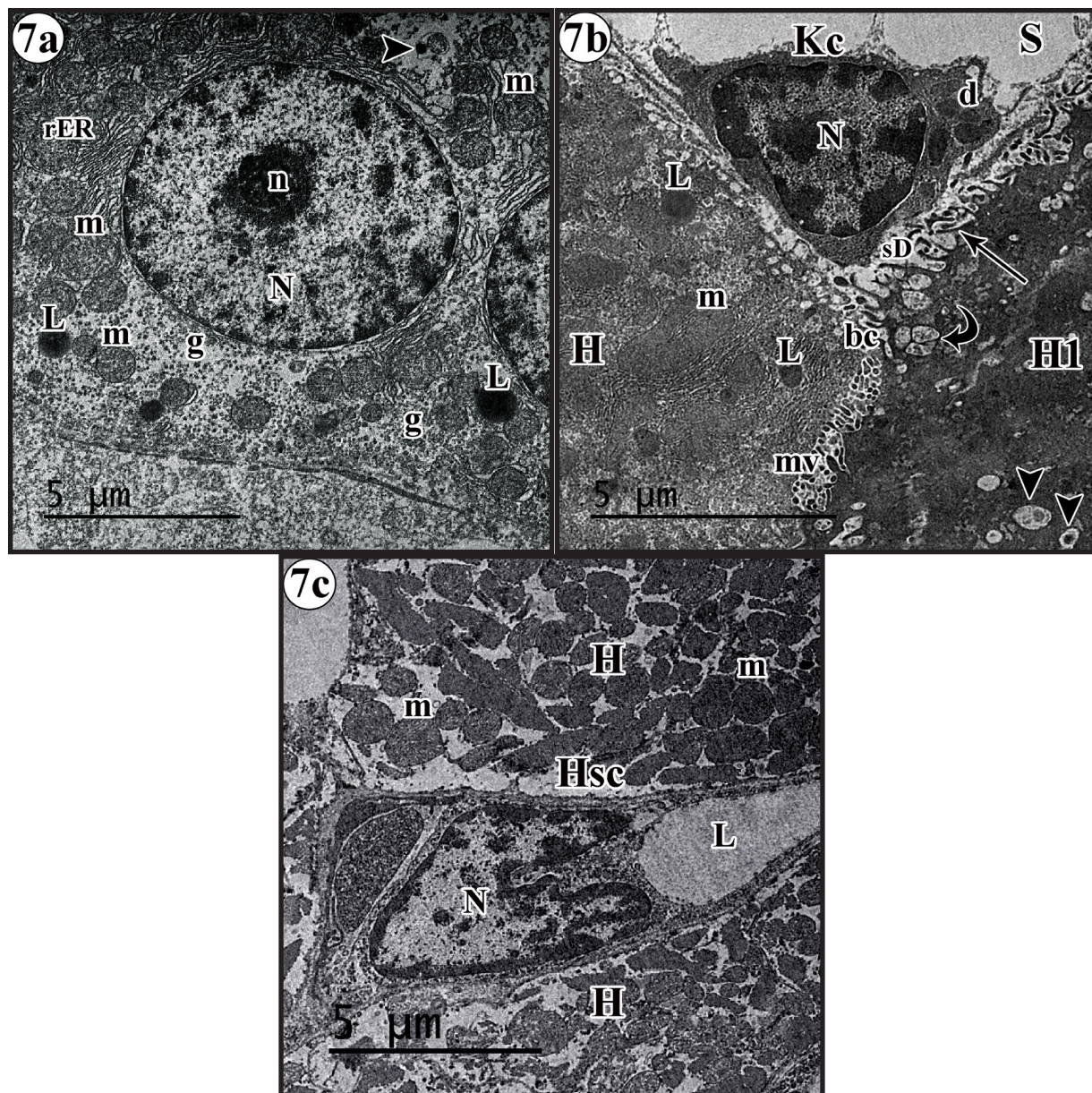


**Fig. 7 (a-c):** Electron micrographs demonstrating the ultrastructural features of the control group: (a) Hepatocyte with a round euchromatic nucleus (N) and prominent nucleolus (n). Its cytoplasm contains numerous mitochondria (m), rough endoplasmic reticulum (rER), autolysosome (arrowhead), glycogen granules (g) and lipid droplets (L). (b) Adjacent hepatocytes (H & H1) enclose a bile canaliculus (bc) containing numerous microvilli (mv). A hepatocyte (H) contains numerous mitochondria (m) and lipid droplets (L), while another (H1) displays electron dense cytoplasm, multivesicular bodies (curved arrow) and autophagosomes (arrowhead). A Von Kupffer cell (Kc) with heterochromatic nucleus (N) and dense bodies (d) is seen in the sinusoidal lumen (S). Numerous microvilli (arrow) of the hepatocytes are seen in the space of Disse (sD). (c) Elongated hepatic stellate cell (Hsc) with an indented euchromatic nucleus (N) and a large lipid droplet (L) is seen in the vicinity of the hepatocytes (H). Numerous mitochondria (m) are observed in hepatocytes (H). (Mag. a, x 5000; b, x7000; c, x 5,500)

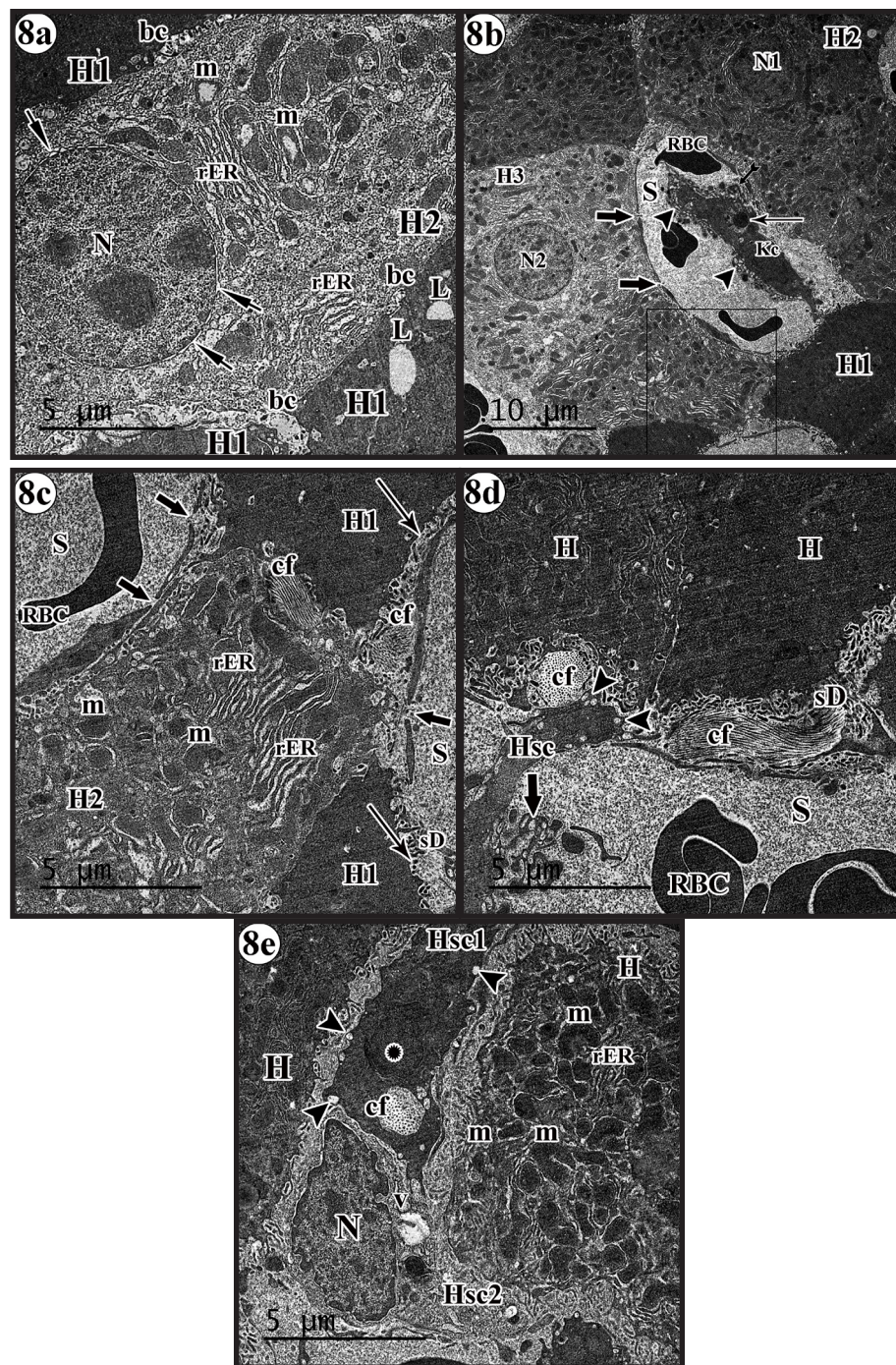


**Fig. 8 (a-e):** Electron micrographs demonstrating the ultrastructural features of the TD group (a) Hepatocytes (H1) have electron dense cytoplasm and lipid droplets (L), whereas (H2) has a nucleus (N) with dilated perinuclear cisterna (short arrow), mitochondria with disrupted cristae (m), dilated cisternae of rough endoplasmic reticulum (rER) and bile canaliculi (bc) with few microvilli. (b) Sinusoidal capillary (S) showing fenestrated endothelium (thick arrow), luminal red blood cells (RBC) and a Von Kupffer cell (Kc) with pseudopodia (tailed arrow), lysosomes (thin arrow) and numerous phagocytic vacuoles (arrowhead). A hepatocyte (H1) possesses an electron dense cytoplasm, while another (H2) has an ill-defined nucleus (N1). Another hepatocyte (H3) displays an electron lucent cytoplasm and euchromatic nucleus (N2). (c) A higher magnification of the boxed area in figure 8 showing parts of a sinusoidal capillary (S) with fenestrated endothelium (thick arrow) and a luminal red blood cell (RBC). The space of Disse (sD) contains few microvilli (thin arrow) and collagen fibers (cf). Collagen fibers (cf) are also observed between the adjacent hepatocytes. Some hepatocytes (H1) have electron dense cytoplasm while another (H2) contains dilated rough endoplasmic reticulum (rER) and mitochondria (m). (d) Hepatocytes with electron dense cytoplasm (H), collagen fibers (cf) in the space of Disse (sD) and a sinusoidal capillary (S) with luminal red blood cells (RBC) are seen. A part of a hepatic stellate cell (Hsc) with numerous long processes (thick arrow) and small lucent vacuoles (arrow head) is present. (e) Hepatic stellate cells (Hsc1 & Hsc2) are seen in the vicinity of adjacent hepatocytes (H). Hsc1 has irregular outline, ill defined, heterochromatic nucleus (asterisk), numerous marginal vacuoles (arrowhead) and collagen fibers (cf) while Hsc2 shows indented euchromatic nucleus (N) and vacuole (v) in its cytoplasm. Hepatocytes (H) with rough endoplasmic reticulum (rER) and dense irregular shaped mitochondria (m) are observed. (Mag. a,c,d,e x6000, b x 3000)

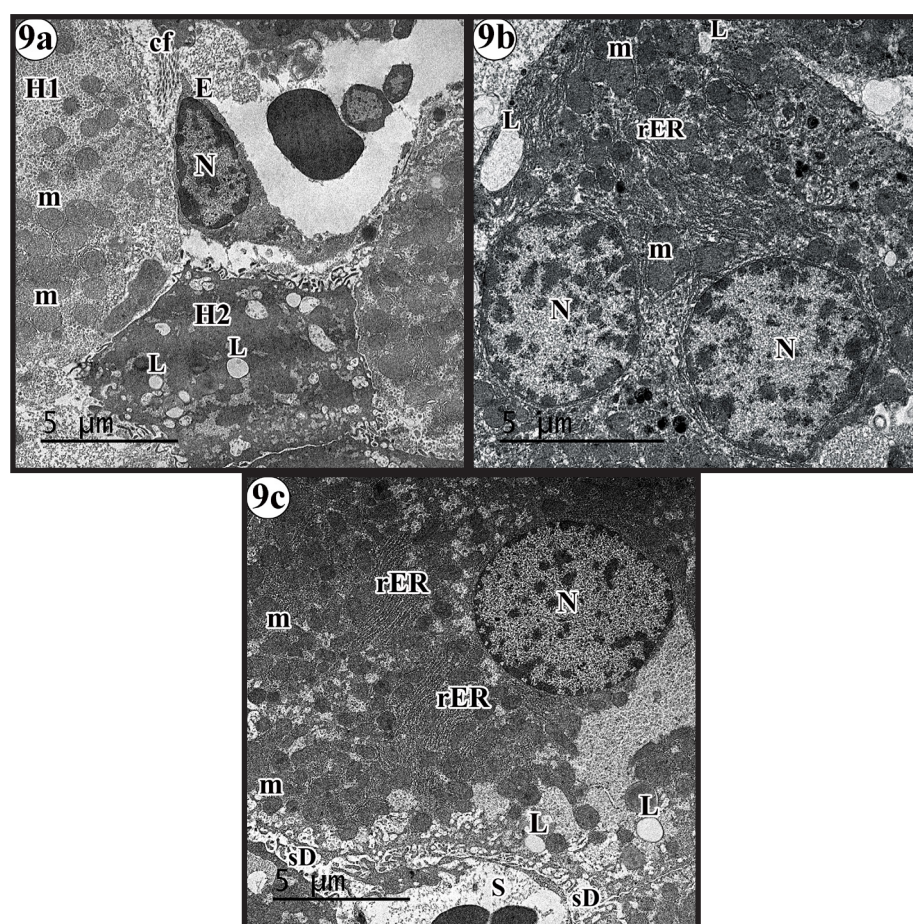


**Fig. 9 (a-c):** Electron micrographs demonstrating the ultrastructural features of the SeNPs + TD group showing (a) A hepatocyte (H1) with numerous mitochondria (m) and another (H2) with electron dense cytoplasm and multiple lipid droplets (L). An endothelial cell (E) is seen with a euchromatic nucleus (N). Collagen fibers (cf) are also observed. (b) A hepatocyte appears binucleated (N) with rough endoplasmic reticulum (rER), mitochondria (m) and few lipid droplets (L). (c) Another hepatocyte appears with euchromatic nucleus (N), rough endoplasmic reticulum (rER), numerous intact mitochondria (m) and small lipid droplets (L). Sinusoidal capillary (S) and numerous microvilli in space of Disse (sD) are also seen. (Mag. a, x 5000; b, x7000; c, x 5,500)

## DISCUSSION

The liver is a predominant organ participating in diverse detoxifying functions. Therefore, sustained exposure to excess levels of endogenous and exogenous oxidants could lead to hepatotoxicity. Despite the well documented antioxidant effects of SeNPs in various drug induced organ toxicities, our study was the first to evaluate its role in TD induced hepatotoxicity.

Tramadol induced oxidative stress in the present study was clearly evidenced by a significant down-regulation in the antioxidant enzyme activities (CAT, SOD and GPx). Similar findings were reported owing to exhaustion of enzyme activity due to the over production of reactive oxygen species (ROS) induced by tramadol administration<sup>[32,33]</sup> Also, possible damage of these enzymes may have occurred through the byproducts of lipid peroxidation.<sup>[34]</sup> Oxidative stress represents the imbalance between reactive oxygen species (ROS) generation and its effective elimination by both enzymatic and nonenzymatic antioxidants.<sup>[35]</sup> Accumulation of ROS lead to the damage of cellular lipids, proteins, and DNA along with activation of proapoptotic pathways.<sup>[36,37]</sup>

MDA levels were also significantly increased in the TD treated group. This finding is of interest, since MDA is a sensitive marker of lipid peroxidation and is widely used to measure oxidative stress.<sup>[38]</sup> Membranes of cells and organelles are particularly susceptible to attack by ROS, due to their rich polyunsaturated fatty acids. This results in lipid peroxidation leading to the production of MDA.<sup>[39]</sup> In agreement with our findings, chronic tramadol administration was reported to significantly increased ROS resulting in increased MDA level and suppressed SOD activity. MDA induces further damage to phospholipids, nucleic acids, and proteins, ultimately resulting in cell death.<sup>[40]</sup>

In our study, oxidative stress induced damage of the hepatocyte structure and function manifested biochemically as a significant elevation of serum ALT, AST, and ALP levels with a significant reduction in total proteins and albumin. Similar changes in liver enzymes have been recorded in previous experiments.<sup>[8,41]</sup> They attributed this impairment to leakage of the previously mentioned biomarkers into the plasma following an increased permeability of the hepatocyte cell membrane secondary to lipid peroxidation.<sup>[42]</sup> This is in line with the increased

MDA level observed in the current study. The observed reduction in total proteins and albumin levels may indicate compromised hepatic synthetic activity as these substances are primarily produced by the liver.<sup>[43]</sup>

Oxidative stress leads to cellular injury and ultimately cell death. Additionally, impairment of the liver's antioxidant enzyme activity is intimately related to the initiation and progression of many liver diseases.<sup>[44]</sup> Histologically, Group III (TD group) revealed evident alteration of hepatic structures. Congested dilated central veins and sinusoids in addition to swollen hepatocytes with extensive cytoplasmic rarefaction and darkly stained nuclei were observed. Inflammatory cells were also present near the central veins and in the portal areas. Our findings are in line with those reported by previous authors.<sup>[45,46]</sup> Consistent with our biochemical and histological findings, byproducts of lipid peroxidation have been reported to act as a triggers for cell death and inflammation.<sup>[39]</sup> Additionally, the cytoplasmic changes have been attributed to disturbance of hepatic lipid metabolism.<sup>[47]</sup>

Histochemically, hepatocytes of the tramadol treated group demonstrated a highly significant depletion of their intracellular protein content in mercuric bromophenol blue sections when compared to the other groups. Our finding was also observed in a previous study. In addition to attacking lipids, oxidative stress leads to a plethora of damaging effects on proteins.<sup>[41]</sup> This includes amino acid alterations, breakage in peptide chains and cross-linking of proteins altering their structure and function.<sup>[48]</sup> The resultant oxidized proteins have a higher susceptibility to proteolytic elimination by proteasomes.<sup>[49]</sup> This mechanism is supported by the decline in antioxidant enzyme activity and increased MDA level observed in this study. Furthermore, a significant decrease in glycogen content was also observed. This was in line with findings of a novel study that explained this reduction secondary to increased glycolysis.<sup>[47]</sup>

Immunohistochemically, the TD treated group demonstrated a significant increase in Bax and GFAP immune expression when compared to the other groups. Furthermore, a negative Pearson's correlation was observed between antioxidant enzyme activity and Bax and GFAP immune expression. On the other hand, a positive correlation was observed between MDA levels and Bax and GFAP immune expression. A Similar upregulation of Bax expression associated with decline in antioxidant enzyme activity and increased MDA level was recorded. They explained that oxidative stress induces apoptosis through an upregulation of pro-apoptotic markers p53 and Bax and down regulation of anti-apoptotic Bcl2 expression. This increased Bax immune expression may partly explain the degenerative changes observed at both light and electron microscope levels. Additionally, a significant increase in the serum levels of pro-inflammatory cytokines including tumor necrosis factor- $\alpha$  (TNF- $\alpha$ ) and interleukin-6 (IL-6) was reported leading to tramadol induced inflammation of the cerebrum in a rat model.<sup>[50,51]</sup>

To the best of our knowledge, no previous studies evaluating TD hepatotoxicity explicitly reported an increased GFAP immune expression. However, GFAP expression in the hepatic stellate cells (HSCs) is reported to be a marker of early activation following liver injury and prior to the development of fibrosis.<sup>[52]</sup> Hepatic stellate cells are normally quiescent and produce extracellular matrix and collagen fibers. They are only activated during liver injury into myofibroblast like cells that produce excessive amount of collagen leading to fibrosis and subsequent cirrhosis.<sup>[53]</sup> Furthermore, a vascular role for GFAP previously proposed in a stroke model. GFAP expression in activated astrocytes of this model was found to contribute to blood flow regulation after injury.<sup>[54]</sup> The similar expression of GFAP by the HSCs in our model may suggest a role in vascular remodeling and neovascularization observed in liver injury.

Ultrastructurally, TD administration adversely impacted the different hepatic cells. The hepatocytes showed dilated rough endoplasmic reticulum, mitochondria with disrupted cristae, and many lipid droplets. Some nuclei had dilated perinuclear cisternae, while others appeared ill defined with electron dense cytoplasm. Von Kupffer cells in the sinusoidal lumens had pseudopodia, lysosomes, and numerous phagocytic vacuoles. The hepatic stellate cells revealed numerous long processes, irregular outline and ill-defined heterochromatic nuclei. Our findings were consistent with those reported by a previous study<sup>[55]</sup> Excessive ROS reportedly oxidize sulfhydryl groups in proteins causing their misfolding. These misfolded proteins accumulate in the endoplasmic reticulum (ER) causing ER stress and disruption of cellular homeostasis. ER stress triggers the secretion of defective proteins which is associated with increased lipid droplet formation within hepatocytes.<sup>[56]</sup> This explanation is in line with the dilated ER and lipid droplets seen the hepatocytes of the TD treated group. Additionally, the bile canaliculi and space of Disse contained few microvilli. Lipid peroxidation alters the composition, structure, assembly and permeability of membranes, leading to disturbance of normal cellular structure and function.<sup>[57]</sup> ROS also react with mitochondrial lipids, proteins, and DNA.<sup>[58]</sup> Mitochondrial DNA is highly prone to ROS attack due to its deficiency in histones ultimately leading to mitochondrial damage, and release of apoptotic factors.<sup>[59]</sup>

Excessive ROS also interferes with the normal functioning of liver specific cells and triggers the initiation of fibrosis. ROS induce apoptosis and necrosis of the hepatocytes. Additionally, injurious stimuli amplify ROS production by Kupffer cells leading to activation of hepatic stellate cells with excessive extracellular matrix deposition.<sup>[60]</sup> This is in line with collagen deposition observed between the hepatocytes, in the space of Disse, and close to the hepatic stellate cells in the present study.

Administration of SeNPs significantly improved TD induced hepatotoxicity. Biochemically, SeNPs lead to a significant increase in antioxidant enzyme activities.

A similar increase in GPx, SOD and CAT activity and decrease in oxidative stress induced neuronal damage in an Alzheimer model after SeNPs administration was reported<sup>[61]</sup> SeNPs have been found to exert their antioxidant properties via two mechanisms: Directly by acting as a potent free radical scavenger<sup>[62]</sup>, and indirectly by increasing the expression and activity of anti-oxidant seleno-enzymes such as GPx.<sup>[63]</sup> Further studies also demonstrated that selenium may mediate an indirect anti-oxidant effect through the activation of vitamin C and Q10 by seleno-proteins.<sup>[21]</sup>

Amelioration of the antioxidant status leads to elimination of excessive ROS thus protecting cellular lipid and protein macromolecules against oxidative damage<sup>[35]</sup> In line with the improved antioxidant enzyme activity, lipid peroxidation was significantly reduced evidenced by decreased MDA level. SeNPs treated group also revealed a significant decline in liver enzyme levels in addition to a significant increase in total protein and albumin levels indicating a protective effect on the hepatocyte cellular membrane. SeNPs inhibited lipid peroxidation in a model of acute kidney injury suggesting its membrane protective effect.<sup>[22]</sup> Furthermore, the hepatocyte protein content was restored after SeNPs administration. Selenoproteins have been reported to protect cellular proteins against oxidative damage.<sup>[64]</sup>

SeNPs also improved the hepatic structure. Most hepatocytes showed vesicular nuclei, acidophilic cytoplasm and organelles similar to those of the control group. Protein content of the hepatocytes was also restored. Selenium is intimately involved in the liver's antioxidant defense system protecting it against oxidative stress. Many studies have demonstrated that in addition to boosting antioxidant enzyme activity, Se supplementation diminishes ROS generation, and reduces the cellular damage.<sup>[62]</sup> Amelioration of oxidative stress induced structural alterations by SeNPs were also observed in diabetic nephropathy and pancreatopathy.<sup>[65]</sup> SeNPs effectively neutralize byproducts of lipid peroxidation thus attenuating damage of hepatocyte and organelle membranes and DNA damage thus preventing apoptosis induced cellular death.<sup>[66]</sup> Additionally, a significant decrease in Bax and GFAP immune expression with an associated reduction in collagen fiber deposition was also observed. A decreased hippocampal neuronal apoptosis was also reported through suppression of the pro-apoptotic marker Bax and increase in anti-apoptotic marker Bcl2 expression.<sup>[67]</sup> SeNPs were also found to downregulated Bax gene expression ameliorating cardiac and hepatic damage secondary to diabetes mellitus<sup>[68]</sup> Furthermore, a decline in hippocampal GFAP expression in cyclophosphamide induced neurotoxicity treated with SeNPs was also documented.<sup>[69]</sup>

## CONCLUSION

SeNPs alleviated TD induced hepatotoxicity through amelioration of antioxidant enzyme activities which attenuated oxidative stress. This protected cellular macromolecules from oxidative injury evidenced by

reduced MDA levels, and restoration of hepatocyte glycogen and protein content. Additionally, reduced BAX and GFAP immune expression protected the liver against cellular death and prevented the progression of fibrosis. Accordingly, the administration of SeNPs may be a promising therapy against the adverse effects of long term TD therapy in patients suffering from chronic pain and/or TD abuse. Further molecular studies are recommended to shed more light on the mechanisms of the hepatoprotective potential of SeNPs.

## CONFLICT OF INTERESTS

There are no conflicts of interest.

## REFERENCES

1. Subedi M, Bajaj S, Kumar MS, Mayur Y. An overview of tramadol and its usage in pain management and future perspective. *Biomed Pharmacother* [Internet]. 2019;111:443–51. Available from: <http://www.embase.com/search/results?subaction=viewrecord&from=export&id=L2001410374%0Ahttp://dx.doi.org/10.1016/j.biopha.2018.12.085>
2. Pergolizzi JV, LeQuang JA, Taylor R, Ossipov MH, Colucci D, Raffa R. Designing safer analgesics: a focus on  $\mu$ -opioid receptor pathways. *Expert Opin Drug Discov*. 2018;13(10):965–72.
3. Mohammadpour A, Ashkezari MD, Behrokh F, Mohammad S. Demographic Characteristics and Functional Performance of the Kidneys and Hearts of Patients with Acute Tramadol Toxicity. *Drug Res (Stuttg)* [Internet]. 2019;69(4):207–10. Available from: <http://www.embase.com/search/results?subaction=viewrecord&from=export&id=L623034558%0Ahttp://dx.doi.org/10.1055/a-0646-3918>
4. Ferrari A, Tiraferri I, Palazzoli F, Licata M. Tramadol abuse in a binge pattern in a young depressed woman. *Eur Addict Res* [Internet]. 2014;20(2):82–6. Available from: <http://www.embase.com/search/results?subaction=viewrecord&from=export&id=L603804524%0Ahttp://dx.doi.org/10.1159/000353971>
5. Skipper GE, Fletcher C, Rocha-Judd R, Brase D. Tramadol abuse and dependence among physicians. *J Am Med Assoc* [Internet]. 2004;292(15):1818–9. Available from: <http://eutils.ncbi.nlm.nih.gov/entrez/eutils/elink.fcgi?dbfrom=pubmed&id=15855429&retmode=ref&cmd=prlinks%5Cnpapers3://publication/doi/10.1001/jama.293.16.1977-a>
6. Ryan NM and Isbister GK. Tramadol overdose causes seizures and respiratory depression but serotonin toxicity appears unlikely. *Clin Toxicol*. 2015;53(6):545–50.
7. Jeong S, Tchoe HJ, Li J, Shin J-Y. All-Cause Mortality Associated with Tramadol Use: A Case-Crossover Study. *Drug Saf* [Internet]. 2019;42(6):785–96. Available from: <http://www.embase.com/search/results?subaction=viewrecord&from=export&id=L625903066%0Ahttp://dx.doi.org/10.1007/s40264-018-00786-y>

8. Barbosa J, Faria J, Leal S *et al.* Acute administration of tramadol and tapentadol at effective analgesic and maximum tolerated doses causes hepato- and nephrotoxic effects in Wistar rats. *Toxicology*. 2017;389:118–29.
9. Baghishani F, Mohammadipour A, Hosseinzadeh H, Hosseini M, Ebrahimzadeh-Bideskan A. The effects of tramadol administration on hippocampal cell apoptosis, learning and memory in adult rats and neuroprotective effects of crocin. *Metab Brain Dis*. 2018;33(3):907–16.
10. Abdel-Salam OM, Youness ER, Mohammed NA, Abd El-Moneim OM, and Shaffie N. Citicoline Protects against Tramadol-Induced Oxidative Stress and Organ Damage. *React Oxyg Species*. 2019;
11. Xu D, Xu M, Jeong S, Qian Y, Wu H, Xia Q *et al.* The role of Nrf2 in liver disease: Novel molecular mechanisms and therapeutic approaches. *Front Pharmacol*. 2019;9(JAN).
12. Skalickova S, Milosavljevic V, Cihalova K, Horky P, Richtera L, and Adam V. Selenium nanoparticles as a nutritional supplement. *Nutrition*. 2017;33:83–90.
13. Malhotra S, Welling MN, Mantri SB, and Desai K. *In vitro* and *in vivo* antioxidant, cytotoxic, and anti-chronic inflammatory arthritic effect of selenium nanoparticles. *J Biomed Mater Res - Part B Appl Biomater*. 2016;104(5):993–1003.
14. Maiyo F and Singh M. Selenium nanoparticles: Potential in cancer gene and drug delivery. *Nanomedicine*. 2017;12(9):1075–89.
15. Rezaei-Kelishadi M, Ghasemi A, Abdolyosefi NN, Zamani-doabi S, Ramezani M, Changizi-Ashtiyani S *et al.* Effects of selenium nanoparticles on kidney and liver functional disorders in streptozotocin-induced diabetic rats. *Physiol Pharmacol*. 2017;21(2):155–62.
16. Dos Santos M., da Silva FM., and Muccillo-Baisch A. Selenium content of Brazilian foods: A review of the literature values. *J Food Compos Anal*. 2017;58:10–5.
17. Urbankova L, Horky P, Skladanka J, Pribilova M, Smolikova V, Nevrkla P *et al.* Antioxidant status of rats' blood and liver affected by sodium selenite and selenium nanoparticles. *PeerJ*. 2018; 6: e4862.
18. Hamza RZ, Al-Motaan S, Shaden E, and Malik N. Protective and Antioxidant Role of Selenium Nanoparticles and Vitamin C Against Acrylamide Induced Hepatotoxicity in Male Mice. *Int J Pharmacol*. 2019;15(6):664–74.
19. Amin KA, Hashem KS, Alshehri F S, Awad ST, Hassan MS. Antioxidant and Hepatoprotective Efficiency of Selenium Nanoparticles Against Acetaminophen-Induced Hepatic Damage. *Biol Trace Elem Res*. 2017;175(1):136–45.
20. Krishnan V, Loganathan C, and Thayumanavan P. Green synthesized selenium nanoparticles using *Spermacoce hispida* as carrier of s-allyl glutathione: to accomplish hepatoprotective and nephroprotective activity against acetaminophen toxicity. *Artif Cells, Nanomedicine Biotechnol*. 2019;47(1):56–63.
21. Khurana A, Tekula S, Saifi MA, Venkatesh P, and Godugu C. Therapeutic applications of selenium nanoparticles. *Biomed Pharmacother* [Internet]. 2019;111:802–12. Available from: <http://www.embase.com/search/results?subaction=viewrecord&from=export&id=L2001435828%0Ahttp://dx.doi.org/10.1016/j.biopha.2018.12.146>
22. AlBasher G, Alfarraj S, Alarifi S, Alkhtani S, Almeer R, Alsultan N, Alharthi M, Alotibi N, Al-dbass A, Abdel Moneim A. Nephroprotective Role of Selenium Nanoparticles Against Glycerol-Induced Acute Kidney Injury in Rats. *Biol Trace Elem Res*. 2020;194(2):444–54.
23. Atici S, Cinel I, Cinel L, Doruk N, Eskandari G, and Oral U. Liver and kidney toxicity in chronic use of opioids: An experimental long term treatment model. *J Biosci*. 2005;30(2):245–52.
24. Aghili H, Moghadam MG, Yassaei S, Meybodi ARF, Tabatabaei SMA. Effect of tramadol at different doses on orthodontic tooth movement and bone resorption in rats. *Dent Res J (Isfahan)* [Internet]. 2013;10(3):337–42. Available from: <http://www.ncbi.nlm.nih.gov/pubmed/24019801%0Ahttp://www.pubmedcentral.nih.gov/articlerender.fcgi?artid=PMC3760356>
25. Paglia D and Valentine W. Studies on the quantitative and qualitative characterization of erythrocyte glutathione peroxidase. *J Lab Clin Med*. 1967;70(1):158–69.
26. Aebi H. *Methods of Enzymatic Analysis*. second edi. Vol. 58. Elsevier; 1975. 1085–1085 p.
27. Misra HP and Fridovich I. The role of superoxide anion in the autoxidation of epinephrine and a simple assay for superoxide dismutase. *J Biol Chem*. 1972;247(10):3170–5.
28. Ohkawa H, Ohishi N, and Yagi K. Assay for lipid peroxides in animal tissues by thiobarbituric acid reaction. *Anal Biochem*. 1979;95(2):351–8.
29. Bancroft JD and Gamble M. *Bancroft's theory and practice of histological techniques*. 6th Editio. Vol. 28, Pathology. Philadelphia: Churcill Livingstone; 2013. 381 p.
30. Mazia D, Brewer P, and Affert M. the Cytochemical Staining and Measurement of Protein With Mercuric Bromphenol Blue. *Biol Bull*. 1953;104(1):57–67.
31. Boumendil J, Ehret G, and Laub D. *Sample Preparation*

- Handbook for Transmission Electron Microscopy. Springer, New York; 2010. 338 p.
32. Sadek KM, Lebda MA, Abouzed T K, Nasr SM, El-Sayed Y. The molecular and biochemical insight view of lycopene in ameliorating tramadol-induced liver toxicity in a rat model: implication of oxidative stress, apoptosis, and MAPK signaling pathways. *Environ Sci Pollut Res.* 2018;25(33):33119–30.
  33. Łuczaj W, Gęgotek A, and Skrzydlewska E. Antioxidants and HNE in redox homeostasis. *Free Radic Biol Med.* 2017;111:87–101.
  34. Maciejczyk M, Skutnik-Radziszewska A, Zieniewska I, Matczuk J, Domel E, Waszkiel D *et al.* Antioxidant defense, oxidative modification, and salivary gland function in an early phase of cerulein pancreatitis. *Oxid Med Cell Longev.* 2019;2019.
  35. Su LJ, Zhang JH, Gomez H *et al.* Reactive Oxygen Species-Induced Lipid Peroxidation in Apoptosis, Autophagy, and Ferroptosis. *Oxid Med Cell Longev.* 2019;2019.
  36. Arroyave-Ospina JC, Wu Z, Geng Y, Moshage H. Role of oxidative stress in the pathogenesis of non-alcoholic fatty liver disease: Implications for prevention and therapy. *Antioxidants.* 2021;10(2):1–25.
  37. Tsikas D. Assessment of lipid peroxidation by measuring malondialdehyde (MDA) and relatives in biological samples: Analytical and biological challenges. *Anal Biochem.* 2017;524:13–30.
  38. Que X, Hung MY, Yeang C, Gonen A, Prohaska TA, Sun X *et al.* Oxidized phospholipids are proinflammatory and proatherogenic in hypercholesterolaemic mice. *Nature.* 2018;558(7709):301–6.
  39. Xia W, Liu G, Shao Z *et al.* Toxicology of tramadol following chronic exposure based on metabolomics of the cerebrum in mice. *Sci Rep.* 2020;10(1).
  40. Awadalla EA and Salah-Eldin A-E. Histopathological and Molecular Studies on Tramadol Mediated Hepato-Renal Toxicity in Rats. *IOSR J Pharm Biol Sci.* 2015;10(6):90–102.
  41. Adikwu E and Bokolo B. Melatonin and n-acetylcysteine as remedies for tramadol-induced hepatotoxicity in albino rats. *Adv Pharm Bull.* 2017;7(3):367–74.
  42. Yang X, Schnackenberg LK, Shi Q, Salminen W. Hepatic toxicity biomarkers. *Biomarkers Toxicol.* 2014;241–59.
  43. Li S, Tan HY, Wang N, Zhang ZJ, Lao L, Wong CW, Feng Y. The role of oxidative stress and antioxidants in liver diseases. *Int J Mol Sci.* 2015;16(11):26087–124.
  44. Albarakai AY and Abd Elrhman Alsbery H. Evaluation of the hepatoprotective efficacy of *Moringa oleifera* on tramal-induced liver toxicity in animal modules. *Res J Pharm Biol Chem Sci.* 2016;7(5):1494–501.
  45. Al-Mashhadane FA, Khaleel H, Saidya AMA. Histopathological effects of chronic use of tramadol on liver and kidney in sheep model. *J Pharm Sci Res.* 2019;11(6):2208–12.
  46. Barbosa J, Faria J, Garcez F, Leal S, Afonso LP, Nascimento AV *et al.* Repeated administration of clinical doses of tramadol and tapentadol causes hepato-and nephrotoxic effects in wistar rats. *Pharmaceuticals.* 2020;13(7):1–36.
  47. Hawkins CL and Davies M. Detection, identification, and quantification of oxidative protein modifications. *J Biol Chem.* 2019;294(51):19683–708.
  48. Raynes R, Pomatto LCD, and Davies K. Degradation of oxidized proteins by the proteasome: Distinguishing between the 20S, 26S, and immunoproteasome proteolytic pathways. *Mol Aspects Med.* 2016;50:41–55.
  49. Ibrahim M and Salah-Eldin A. Chronic addiction to tramadol and withdrawal effect on the spermatogenesis and testicular tissues in adult male albino rats. *Pharmacology.* 2019;103(3–4):202–11.
  50. Mohamed HM and Mahmoud A. Chronic exposure to the opioid tramadol induces oxidative damage, inflammation and apoptosis, and alters cerebral monoamine neurotransmitters in rats. *Biomed Pharmacother* [Internet]. 2019;110:239–47. Available from: <http://www.embase.com/search/results?subaction=viewrecord&from=export&id=L2001339952%0Ahttp://dx.doi.org/10.1016/j.biopha.2018.11.141>
  51. Morini S, Carotti S, Carpino G, Franchitto A, Corradini SG, Merli M *et al.* GFAP expression in the liver as an early marker of stellate cells activation. *Ital J Anat Embryol.* 2005;110(4):193–207.
  52. Li J, Zhao Y, and Tian Z. Roles of hepatic stellate cells in acute liver failure: From the perspective of inflammation and fibrosis. *World J Hepatol.* 2019;11(5):412–20.
  53. Zhang S, Wu M, Peng C, Zhao G and Gu R. GFAP expression in injured astrocytes in rats. *Exp Ther Med.* 2017;14(3):1905–8.
  54. Omar NM and Mohammed M. The impact of black seed oil on tramadol-induced hepatotoxicity: Immunohistochemical and ultrastructural study. *Acta Histochem.* 2017;119(5):543–54.
  55. Fujii J, Homma T, Kobayashi S, and Seo H. Mutual interaction between oxidative stress and endoplasmic reticulum stress in the pathogenesis of diseases specifically focusing on non-alcoholic fatty liver disease. *World J Biol Chem.* 2018;9(1):1–15.
  56. Gaschler MM and Stockwell B. Lipid peroxidation in cell death. *Biochem Biophys Res Commun.* 2017;482(3):419–25.
  57. Dan Dunn J, Alvarez LAJ, Zhang X, and Soldati T.

- Reactive oxygen species and mitochondria: A nexus of cellular homeostasis. *Redox Biol.* 2015;6:472–85.
58. Bouchez C and Devin A. Mitochondrial Biogenesis and Mitochondrial Reactive Oxygen Species (ROS): A Complex Relationship Regulated by the cAMP/PKA Signaling Pathway. *Cells.* 2019;8(4):287.
  59. Luangmonkong T, Suriguga S, Mutsaers HAM, Groothuis GMM, Olinga P, Boersema M. Targeting oxidative stress for the treatment of liver fibrosis. *Rev Physiol Biochem Pharmacol.* 2018;175:71–102.
  60. Nazıroğlu M, Muhamad S, Pecze L. Nanoparticles as potential clinical therapeutic agents in Alzheimer's disease: focus on selenium nanoparticles. *Expert Rev Clin Pharmacol.* 2017;10(7):773–82.
  61. Zhai X, Zhang C, Zhao G, Stoll S, Ren F, and Leng X. Antioxidant capacities of the selenium nanoparticles stabilized by chitosan. *J Nanobiotechnology.* 2017;15(1).
  62. Bai K, Hong B, He J, Hong Z, and Tan R. Preparation and antioxidant properties of selenium nanoparticles-loaded chitosan microspheres. *Int J Nanomedicine.* 2017;12:4527–39.
  63. Steinbrenner H, Speckmann B, and Klotz L. Selenoproteins: Antioxidant selenoenzymes and beyond. *Arch Biochem Biophys.* 2016;595:113–9.
  64. Hassan I, Ebaid H, Al-Tamimi J, Habila MA, Alhazza IM, Rady A. Selenium nanoparticles mitigate diabetic nephropathy and pancreatopathy in rat offspring via inhibition of oxidative stress. *J King Saud Univ - Sci.* 2021;33(1).
  65. Lesnichaya M, Karpova E, and Sukhov B. Effect of high dose of selenium nanoparticles on antioxidant system and biochemical profile of rats in correction of carbon tetrachloride-induced toxic damage of liver. *Colloids Surfaces B Biointerfaces.* 2021;197.
  66. Yuan X, Fu Z, Ji P, Guo L, Al-Ghamdy AO, Alkandiri A, *et al.* Selenium nanoparticles pre-treatment reverse behavioral, oxidative damage, neuronal loss and neurochemical alterations in pentylenetetrazole-induced epileptic seizures in mice. *Int J Nanomedicine.* 2020;15:6339–53.
  67. Mohamed AAR, Khater SI, Hamed AA, Metwally MMM, Mostafa-Hedeab G, El-Shetry E. Chitosan-stabilized selenium nanoparticles alleviate cardio-hepatic damage in type 2 diabetes mellitus model via regulation of caspase, Bax/Bcl-2, and Fas/FasL-pathway. *Gene.* 2021;768.
  68. Ibrahim HM, Zommara MAE, and Elnaggar M. Ameliorating effect of selenium nanoparticles on cyclophosphamide induced hippocampal neurotoxicity in male rats: light, electron microscopic and immunohistochemical study. *Folia Morphol (Warsz).* 2020; Oct 21. doi: 10.5603/FM.a2020.0117. Online ahead of print.

## الملخص العربي

### تأثير جزيئات النانوسيلينيوم على السمية الكبدية المستحثة بالترامادول في نموذج الجرذ

أريج أمير كمال دسوقي<sup>١</sup>، منال رضا عبد الحليم<sup>١</sup>، مصطفى محمد إبراهيم مصطفى<sup>٢</sup>، نهى محمد هلول<sup>٣</sup>،  
إيمان محمد عسكر<sup>١</sup>

<sup>١</sup>قسم الهستولوجيا الطبية وبيولوجيا الخلية - كلية الطب-جامعة الزقازيق

<sup>٢</sup>مستشفى ماتر-دبلن-ايرلندا

<sup>٣</sup>قسم الطب الشرعي والسموم- كلية الطب-جامعة الزقازيق

**المقدمة:** تعتبر جزيئات النانوسيلينيوم علاجًا واعدًا للعديد من الأمراض الناجمة عن الإجهاد التأكسدي والالتهاب. يعتبر الترامادول أكثر المواد الأفيونية الموصوفة شيوعًا مع وجود احتمالية عالية للإدمان ، مما يؤدي إلى السمية الكبدية نتيجة للإجهاد التأكسدي.

**الهدف من الدراسة:** تهدف هذه الدراسة إلى توضيح تأثير جزيئات النانوسيلينيوم على التغيرات الكيميائية الحيوية والهستولوجية التي يسببها الترامادول.

**المواد والطرق:** تم تقسيم ستين جرذا إلى أربعة مجموعات: المجموعة الأولى (١٥ جرذا): المجموعة الضابطة ، المجموعة الثانية (٥ جرذان): تلقت جزيئات النانوسيلينيوم ، المجموعة الثالثة (٢٠ جرذا): تلقت الترامادول، المجموعة الرابعة (٢٠ جرذا) : تلقت جزيئات النانوسيلينيوم + الترامادول. تمت معالجة عينات الكبد للدراسات البيوكيميائية والضوء والمجهرية الإلكترونية والتحليل المورفومتري والإحصائي.

**النتائج:** أدى تعاطى الترامادول لخفض نشاط الإنزيمات المضادة للأكسدة وارتفاع مستويات إنزيمات الكبد والمالونديالديهيد. كما لوحظ توسع واحتقان الأوردة المركزية والجيوب الكبدية وتضخم خلايا الكبد مع انوية متقلصة غامقة وسيتوبلازم النادر وتسلل التهابي. كان هذا مرتبطًا بنقص الجليكوجين والبروتينات داخل الخلايا، وزيادة التعبير المناعي لل Bax و GFAP ، وترسب الكولاجين بالقرب من الخلايا النجمية الكبدية ، وبين خلايا الكبد ، وفي مسافات ديس. حسنت جزيئات النانوسيلينيوم هذه التغيرات على الأرجح بسبب خصائصها المضادة للأكسدة.

**الخلاصة:** أدت جزيئات النانوسيلينيوم إلى تحسين الآثار الضارة الناتجة عن تعاطى الترامادول في كبد الجرذان والتي قد تكون بسبب خصائصها المضادة للأكسدة.